ISSN (Print) 1226-1750
ISSN (Online) 2233-6656
Journal of Magnetics 31(3), 340-357 (2026) https://doi.org/10.4283/JMAG.2026.31.3.340

A Multicenter Survey and Practical Recommendations for Establishing Magnetic Resonance Imaging Protocol Guidelines for Gamma Knife Radiosurgery in Korea

Kyung-Bae Lee[1†], Jun-Ho Hwang[2†], Gi-Hong Kim[3], Byungmok Kim[4], Doheui Lee[5,6], Hyun-Ji Lee[3], Sa-Hoe Lim[7,8], Yong-Seok Im[9], Seok Keun Choi[2,10], and Chang Kyu Park[2,10]*

[1]Department of Radiological Science, Wonkwang University, Iksan 54538, Republic of Korea
[2]Department of Neurosurgery, Kyung Hee University Medical Center, Seoul 02447, Republic of Korea
[3]Department of Neurosurgery, Severance Hospital, Seoul 03722, Republic of Korea
[4]Department of Neurosurgery, Gamma Knife Center, Kyungpook National University Hospital, Daegu 41944, Republic of Korea
[5]Radiosurgery Center, Asan Medical Center, University of Ulsan College of Medicine, Seoul 05505, Republic of Korea
[6]Department of Neurosurgery, Asan Medical Center, Seoul 05505, Republic of Korea
[7]Department of Neurosurgery, Chonnam National University Medical School, Hwasun 58128, Republic of Korea
[8]Department of Neurosurgery, Chonnam National University Hwasun Hospital, Hwasun 58128, Republic of Korea
[9]Department of Neurosurgery, Samsung Medical Center, Seoul 06351, Republic of Korea
[10]Department of Neurosurgery, Kyung Hee University College of Medicine, Seoul 02447, Republic of Korea

(Received 20 April 2026, Received in final form 2 September 2026, Accepted 2 September 2026)

This study aimed to compare and analyze the magnetic resonance imaging (MRI) parameters used for gamma knife radiosurgery (GKRS) in Korea and to propose the direction of a practical domestic MRI guideline for GKRS. The study methods involved reviewing recommendations from international organizations applicable to stereotactic radiosurgery (SRS) and GKRS, and, based on these recommendations, comprehensively examining both the aspects emphasized by international organizations and the detailed MRI techniques considered important in the domestic clinical setting. Domestic MRI protocols were systematically investigated according to three categories: tumor, vascular, and nerve protocols. Based on these criteria, the evaluation of the domestic multicenter protocols revealed partial compliance with the recommendations for securing physical resolution, largely achieved through the application of thin slice thicknesses and high resolution sequences. However, inter-institutional variations and limitations stemming from different hardware environments were observed, particularly regarding the use of low bandwidth (BW), suboptimal management of post contrast delay times, and the limited utilization of supplementary sequences such as fluid-attenuated inversion recovery (FLAIR). Therefore, to ensure greater clinical consistency, these findings highlight the necessity of establishing tailored standardization guidelines for Korea, such as proposing specific parameters that reflect the domestic clinical environment.

Keywords : gamma knife radiosurgery (GKRS), magnetic resonance imaging (MRI), protocol comparison, guideline recommendation, multicenter survey

1. Introduction

In modern medicine, medical imaging plays an essential and critical role, as the diagnosis of disease and determination of treatment strategies are based on accurate imaging examinations [1–4]. In the field of neurosurgery, the importance of precise medical imaging is even more pronounced. Diseases arising within the cranial cavity can affect the nervous system, which is responsible for vital human functions, and neurosurgery can employ image based three-dimensional surgical techniques to manage these conditions [4–6]. Because the goal of image-guided surgical techniques is to control the disease while preserving normal tissue as much as possible, medical imaging that can clearly distinguish pathological lesions from normal structures is indispensable.

Representative image-based surgical techniques include direct craniotomy and indirect gamma knife radiosurgery (GKRS), which uses radiation; both approaches can utilize

©The Korean Magnetics Society. All rights reserved.
*Corresponding author: Tel: +82-2-958-8385
Fax: +82-2-958-8380, E-mail: changchaz@naver.com
†These authors contributed equally to this work.

© 2026 Journal of Magnetics

magnetic resonance imaging (MRI) to clearly distinguish pathological lesions from normal tissue. MRI is considered a key factor in determining the success of surgical treatment because it provides three-dimensional spatial information while offering excellent soft tissue contrast at high resolution [7].

The application of the treatment modalities is evaluated based on multiple factors. The final treatment strategy is determined through comprehensive consideration of whether the disease is benign or malignant, as well as its location, type, size, and the patient's age. In both approaches, precise imaging techniques are applied to achieve greater surgical accuracy. Direct surgery uses image-guided neurosurgical techniques in which computed tomography (CT) and MRI data are integrated into a computer system to identify the location of the lesion [5]. When the lesion is located in the central nervous system or in functionally critical regions, localization can be extremely time-consuming; image-guided neurosurgical techniques help address this limitation and thereby enable safer surgery. When major postoperative complications are a significant concern, GKRS may be considered as a second treatment option [6].

GKRS is a form of image-guided radiosurgical treatment based on medical imaging. Because GKRS aims to control the disease by prescribing a high radiation dose to the boundary between the lesion and the surrounding normal tissue, MRI is regarded as an essential imaging modality capable of clearly distinguishing the lesion from normal structures [6, 7]. Reflecting this clinical need, since the introduction of GKRS in Korea, individual centers have applied MRI with high spatial resolution using magnetic field strengths ranging from 1.5 tesla (T) to 3.0 T, based on their own institutional judgment [6]. Another important factor for more accurate diagnosis is the diversity of imaging sequences. Because each disease has its own distinctive characteristics, various MRI techniques, including T2 weighted imaging (T2WI), T1 weighted imaging (T1WI), fluid attenuated inversion recovery (FLAIR), and proton density (PD), are used to visualize these unique features radiologically [8–10]. The selection of these techniques is also based on the judgment of each center, and, when necessary, additional MRI sequences may be incorporated into GKRS planning [11-13].

In Korea, MRI acquisition for GKRS has largely been determined by the judgment of individual centers, resulting in inter-center variability in image quality. Moreover, when new centers are established or when MRI systems at existing centers are replaced with newer equipment, maintaining MRI quality above a consistent standard becomes increasingly challenging. In other words, although institutional regulations and guidelines for equipment use are in place, the minimum requirements necessary to maintain a consistent level of MRI quality for GKRS are often determined according to the internal circumstances of each center. For this reason, international organizations have published a range of studies and recommendations addressing parameter optimization to ensure a standardized level of imaging quality [14–20]. Because maintaining a consistent level of image quality has a substantial impact on GKRS outcomes, collecting the characteristic practices of individual centers and establishing standardized settings could greatly contribute to the success of GKRS. Accordingly, this study aimed to describe and comprehensively analyze the configurations and parameter setting ranges of MRI protocols currently used for GKRS planning across domestic centers. By comparing these findings with international recommendations to identify areas requiring standardization, we sought to go beyond a simple descriptive survey and propose a direction for practical guidelines applicable to clinical settings. However, it should be noted that as a multicenter survey, this study was not designed to directly verify the image quality, geometric accuracy, target delineation accuracy, or clinical superiority of specific MRI protocols.

2. Background

2.1. Magnetic resonance imaging

MRI is a technique that visualizes biologic information required for disease diagnosis by combining magnets, coils, image-processing software, and various pulse sequences [21]. Compared with other medical imaging modalities, MRI offers major advantages in terms of high spatial resolution and superior soft tissue contrast. Accordingly, MRI has continued to evolve toward improving both resolution and contrast, with particularly active advances in magnetic field strength, the number of transmit and receive channels, and examination space design [21–23]. The basic principle of MRI is as follows. MRI generates images by recording signals produced when atomic nuclei resonate in response to a magnetic field and radiofrequency pulses, and hydrogen nuclei in water molecules, a major component of the human body, are used as the primary targets of resonance. Hydrogen has a single positive charge, and when exposed to an external magnetic field, it undergoes precessional motion around a specific axis. When a radiofrequency pulse matching this precessional frequency is applied, the atomic nuclei resonate, and when the external radiofrequency is discontinued, a decay signal is generated.

After this signal is amplified using methods such as spin echo, images can be obtained by recording frequencies from different positions in three-dimensional space.

2.2. Disease diagnosis based on magnetic resonance imaging

Diseases that can occur in the brain include brain tumors, vascular lesions, and functional disorders [24–27]. In neurosurgical practice, diagnosis based on MRI requires careful evaluation of the lesion's location, type, and the presence of neurological symptoms. This is because diseases arising in the brain are problematic not only because of their location and pathological nature, but also because the secondary neurological dysfunction they produce may lead to even more serious consequences. Table 1 shows how various MRI techniques are used in the diagnosis and treatment of these conditions. Among benign tumors, pituitary adenoma, meningioma, and vestibular schwannoma may be accompanied by neurological symptoms [24, 25]. Pituitary adenoma typically arises in the sella turcica. Because the sella turcica is anatomically located close to the optic nerve, compression or involvement of the optic apparatus by a pituitary adenoma may result in neurological symptoms such as diplopia and visual disturbance [24]. In this setting, contrast enhanced T1WI (CE-T1WI) shows lower signal intensity than the normal pituitary parenchyma and clearly delineates the boundary between the lesion and normal tissue within the sella, thereby playing an important role in assessing compression of the optic nerve and its pathway. In patients with tinnitus and hearing loss, meningioma or vestibular schwannoma arising in the cerebellopontine angle (CPA) should be suspected [25]. T2WI and CE-T1WI are the primary sequences to consider, as these lesions typically show higher signal intensity than brain parenchyma on T2WI and strong contrast enhancement on CE-T1WI. In some cases, meningiomas may demonstrate a dural tail sign, whereas vestibular schwannomas may show the ice cream cone sign. Among vascular diseases, cerebral arteriovenous malformation can occur in various brain regions and may cause symptoms such as headache and dizziness [26]. It can be effectively diagnosed using T2WI and time of flight (TOF). On T2WI, arteriovenous malformations may show a dark low-signal nidus, whereas TOF visualizes signal enhancement from unsaturated inflowing blood, thereby clearly depicting high-flow arterial circulation and the nidus. Among functional disorders, trigeminal neuralgia is commonly evaluated using high resolution three-dimensional MRI techniques. One of the causes of trigeminal neuralgia is compression of the trigeminal nerve by adjacent blood vessels, resulting in pain [27]. High resolution three-dimensional MRI can depict neural and vascular structures in great detail, allowing accurate diagnosis of both the location and extent of neurovascular compression by small vessels.

2.3. Gamma knife radiosurgery

GKRS is a form of stereotactic radiosurgery (SRS) that combines the ability to visualize intracranial lesions with the ability to deliver a prescribed dose of radiation precisely to a desired target location [28, 29]. Representative technologies for visualizing intracranial lesions include medical imaging modalities such as CT, MRI, and X-ray, whereas the technology that enables precise radiation delivery refers to a three-dimensional spatial

Table 1. Example for brain diseases and symptoms using MRI methods.

Disease	Location	Symptoms	MRI methods	Features
Pituitary adenoma	Sella	Diplopia, visual disturbance	CE-T1WI	Low signal than pituitary parenchyma
Meningioma	Cerebellar pontine angle	Tinnitus, hearing disturbance	T2WI	High signal than brain parenchyma
			CE-T1WI	Strong contrast enhancement signal, dural tail sign
Vestibular schwannoma			T2WI	High signal than brain parenchyma
			CE-T1WI	Strong contrast enhancement signal Ice cream cone sign
Arteriovenous malformation	Various locations of brain	Dizziness, headache	T2WI	Black low signal
			TOF	Visualizing signal enhancement that occurs as blood unsaturated with a magnetic field flows in
Trigeminal neuralgia	Trigeminal nerve	Sharp and stabbing pain	High resolution 3D MRI technique	Visualize the degree and location of microvascular compression of nerves

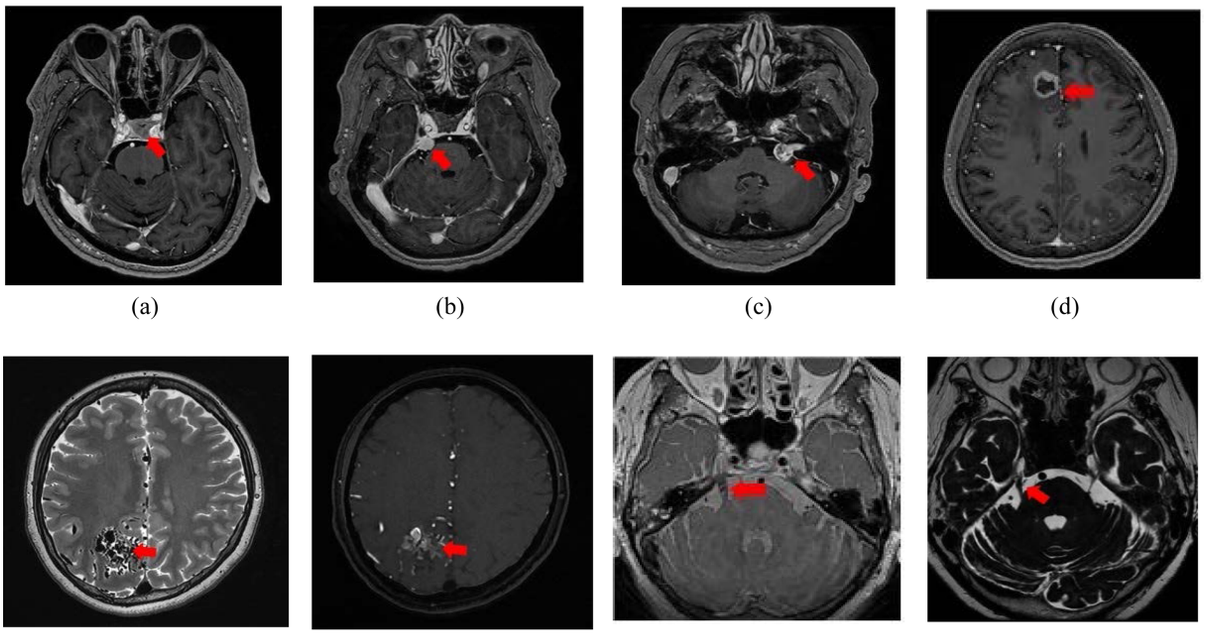


Fig. 1. (Color online) (a)–(h) illustrate the clinical applications of primary MRI sequences used for diagnosing various brain diseases during GKRS planning. The red arrows in each image indicate the lesions clearly identified by the respective MRI sequences. (a) CE-T1WI of a pituitary adenoma, (b) CE-T1WI of a meningioma, (c) CE-T1WI of a vestibular schwannoma, and (d) CE-T1WI of a metastatic brain tumor, clearly delineating the boundaries of each lesion. (e) and (f) present T2WI and TOF images for evaluating the structural characteristics and vascular status of an arteriovenous malformation (AVM). (g) and (h) show PD and high resolution 3D specialized pulse sequence images, utilized to clearly distinguish the anatomical relationship between the trigeminal nerve and surrounding microstructures during the treatment of trigeminal neuralgia.

coordinate system [6, 7, 28–31].

Figure 1 illustrates an example of the use of MRI as an imaging modality for visualizing intracranial lesions. MRI is the imaging technique most commonly used for GKRS because of its ability to clearly depict the anatomical structures of both the lesion and the surrounding normal tissue.

Subsequently, as shown in Fig. 2, GKRS is performed by first establishing the spatial coordinates of the target lesion, either by attaching an indicator that enables coordinate acquisition during imaging or by using the reference cone beam computed tomography (CBCT) function, and then prescribing a radiation dose to the tumor margin sufficient to control the lesion [28, 31].

3. Materials and Methods

3.1. Recommended magnetic resonance imaging protocols by international organizations

First, we examined whether major international organizations provide recommended MRI protocols. Specifically, we investigated items applicable to SRS and GKRS in the guidance or statements issued by the American Association of Physicists in Medicine (AAPM), Radiosurgery Society (RSS), Response Assessment in Neuro-Oncology (RANO), Brain Tumor Imaging Protocol (BTIP), International Stereotactic Radiosurgery Society (ISRS), European Society for Radiotherapy and Oncology (ESTRO), European Association of Neuro-Oncology (EANO), and the German Taskforce.

3.2. Magnetic resonance imaging protocols by domestic institutions

This study included 6 of the 21 institutions performing GKRS in Korea that agreed to participate and were able to provide detailed information on their MRI protocols. The participating institutions were selected via convenience sampling and all consisted of tertiary general hospitals. Geographically, four institutions were located in the Seoul metropolitan area, one in the Gyeongsang-do region, and one in the Jeolla-do region. These 6 centers represent approximately 28.6% (6/21) of all GKRS performing institutions in Korea, with a combined annual GKRS volume of approximately 4,857 cases, accounting for about 60.5% of the total annual cases nationwide. The surveyed MRI systems included those manufactured by

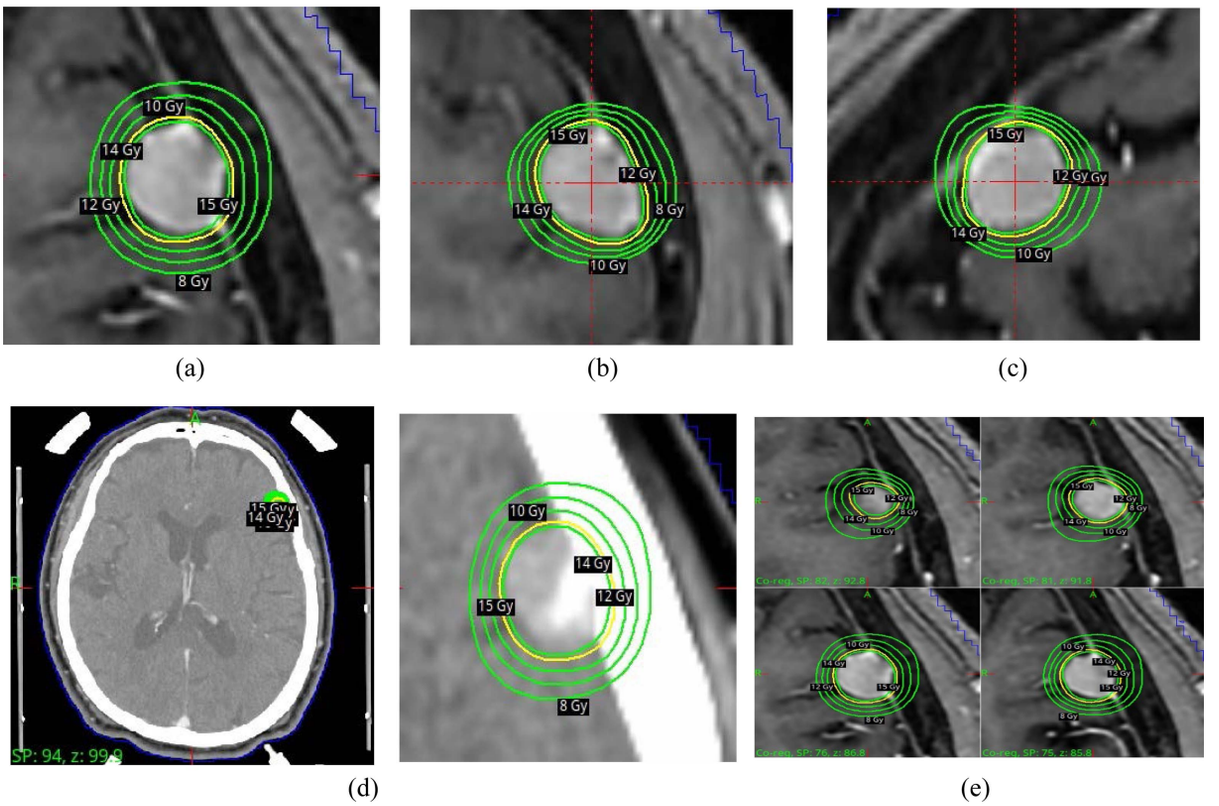


Fig. 2. (Color online) This is an example of GKRS performed using GammaPlan 11.4.2. Panels (a)–(c) show planning MRI obtained to visualize the intracranial lesion, and panel (d) shows an example of coordinate acquisition on CT using the Leksell indicator. Panel (e) demonstrates a practical example of radiosurgical application in which MRI and CT were co-registered, thereby integrating the imaging data with the stereotactic coordinate system.

GE Healthcare, Siemens, and Philips, with magnetic field strengths of 1.5 T and 3.0 T. Furthermore, to reflect the diverse GKRS planning MRI setups utilized in real world domestic clinical settings, both frame-based and frameless environments were included. Specifically, one institution operated exclusively in a frameless environment, two utilized exclusively a frame-based system, and the remaining three employed a combination of both frame-based and frameless environments for MRI examinations.

Data collection was conducted between January and April 2026. A standardized questionnaire consisting of identical items was distributed to all participating institutions, and the protocol survey was completed by a medical physicist stationed at each center's Gamma Knife facility. The scope of the survey was strictly limited to the MRI protocols currently in active clinical use for GKRS at each respective center. In instances where a single institution operated multiple MRI scanners, only the specific scanner utilized for actual radiosurgery planning examinations was included. When multiple MRI protocols existed for a single indication, the sequence routinely employed to evaluate lesion contrast enhancement and peritumoral edema, as well as to ensure accurate target delineation, was selected as the representative protocol.

Specifically, parameters deemed essential for protocol standardization were investigated with reference to the requirements outlined in international guidelines. To objectively evaluate the compliance of the surveyed parameters with these international recommendations, a comparative analysis was conducted using pre-defined key indicators derived from the guideline analysis. These core metrics included thin slice thickness (≤ 1.5 mm), adequate bandwidth (BW) (≥ 440 Hz), the application of imaging sequences for precise targeting, methods of contrast agent utilization, and the degree of parameter matching. The survey was conducted separately for MRI techniques used for tumors, vascular diseases, and neural disorders. Accordingly, the following parameters were examined in detail: MRI equipment, use of a stereotactic frame during MRI acquisition, imaging protocols, magnetic field strength, coil type, patient positioning, BW, phase encoding, pulse sequence, slice thickness, acquisition

matrix, repetition time (TR), echo time (TE), number of excitations (NEX), and flip angle (FA). Relevant parameters were extracted based on the digital imaging and communications in medicine (DICOM) tags of the images. To ensure data reliability, parameter consistency was initially verified by cross-referencing the submitted DICOM tag values with the actual MRI protocol sheets from each institution. Subsequently, a cross-validation process was conducted, in which two researchers independently reviewed the data. Any unidentifiable or missing data points were not arbitrarily adjusted; instead, they were clearly designated as difficulty in verification in the result tables.

4. Results

4.1. Recommended magnetic resonance imaging protocols by international organizations

Analysis of MRI protocol guidelines proposed by international organizations for SRS and clinical brain tumor imaging showed that each guideline specifies the target population, required imaging sequences, and scan parameters. Depending on their intended purpose, these guidelines could largely be categorized into two major directions: ensuring geometric accuracy and maintaining consistency in clinical assessment.

Table 2 presents the details of physics-oriented guidelines focused on geometric precision. The AAPM presents the details of physics-oriented guidelines focused on geometric precision. AAPM stated that MRI can be used for lesion localization, stereotactic localization, and treatment-planning imaging in order to ensure geometric accuracy and minimize errors that may occur during dose calculation. In this context, CT simulation with geometric accuracy and slice thickness appropriate for SRS was addressed, and the use of multimodality image fusion was proposed.

Table 3 summarizes the details of guidelines focused on physical and clinical consistency. RANO 2.0 recommended MRI acquisition based on the BTIP in order to standardize longitudinal treatment response assessment. The BTIP consensus recommended parameter-matched 3D T1WI acquired before and after contrast administration to reduce inter-site and inter-scanner variability in acquisition parameters, and suggested that post-contrast CE-T1WI should be obtained after a fixed delay following contrast injection

Table 2. Recommendations for guidelines in AAPM.

Reference	Target scope and primary objectives	Recommendations	Resolution and key scan parameters
AAPM Report No. 54	Target: SRS Objective: To ensure geometric accuracy and minimize errors in dose calculation	• MRI can be used for target localization and stereotactic definition of the lesion	• Thin contiguous slices for stereotactic imaging
AAPM-RSS MPPG 9.b	Target: SRS Objective: To provide clinical medical physics support for the entire treatment process and ensure appropriate quality assurance and risk management	• MRI data available for planning • CT simulation with appropriate geometric fidelity, spatial resolution, and slice thickness for SRS • Multi-modality image fusion	• Geometric distortion characterization

Table 3. Recommendations for guidelines in RANO 2.0, BTIP consensus.

Reference	Target scope and primary objectives	Recommendations	Resolution and key scan parameters
RANO 2.0	Target: Adult diffuse glioma response assessment in clinical trials Objective: Standardization of longitudinal treatment response evaluation	• Recommended MRI sequences • Standardized MRI acquisition compatible with BTIP recommended • CE-T1WI and T2WI, FLAIR are core sequences for response assessment	• Serial imaging should be performed using consistent acquisition parameters • BTIP-based acquisition is recommended for longitudinal comparability
BTIP consensus	Target: Brain tumor clinical trials Objective: Minimization of inter-scanner and inter-site parameter variability for multicenter data collection	• Parameter-matched pre- and post-contrast 3D T1WI IR-GRE • Axial 2D T2WI and FLAIR • Axial DWI • Optimized scan order to preserve contrast-agent delay before post contrast T1WI	• 3D T1WI: high spatial resolution/ • 2D sequences: thin section acquisition with minimal or no gap when feasible • Compatible with both 1.5 T and 3.0 T scanners • Post contrast T1WI acquired with controlled post contrast timing

to ensure consistency in contrast enhancement assessment. In addition, inversion recovery gradient echo (IR-GRE), 2D T2WI, FLAIR, and diffusion weighted imaging (DWI) were recommended. The guideline also suggested that 2D sequences should be acquired with minimal or no inter-slice gap whenever feasible in order to minimize error, and that the proposed recommendations should be designed to be applicable to both 1.5T and 3.0T systems.

Table 4 summarizes the detailed recommendations of guidelines focused on target optimization and precision. According to the ISRS technical guidelines, thin slice thickness is recommended to improve targeting accuracy for small metastatic lesions, and it is specifically noted that reducing slice thickness from 3 mm to 1.5 mm can significantly improve lesion localization accuracy. The guideline also recommends image acquisition after a fixed delay following contrast administration to achieve optimal lesion definition and suggests that the interval between MRI acquisition and SRS treatment should be kept within 14 days. For lesions adjacent to cranial nerves, additional acquisition of high resolution sequences such as constructive interference in steady state (CISS) or fast imaging employing steady state acquisition (FIESTA) is considered particularly useful. The German Taskforce (DIN 6864-1), in presenting quality criteria for MRI simulation in cranial stereotactic radiotherapy, recommends the use of high resolution CE-T1WI and T2WI. It further advises that the region of interest should be positioned as close as possible to the magnetic field and gradient isocenter to reduce geometric distortion, and recommends setting the BW to at least 440 Hz to minimize distortion caused by B0 inhomogeneity and chemical shift. The ESTRO-EANO guidelines recommend that pretreatment MRI be obtained within 2 weeks before the start of radiotherapy in order to ensure consistency and accuracy in radiotherapy planning. They also suggest that MRI should be acquired, whenever possible, in a position similar to that used during actual treatment, and that CT simulation images should be fused with MRI to improve the accuracy of target and normal tissue delineation. In addition, these guidelines emphasize the importance of maintaining consistency between diagnostic MRI and treatment planning MRI.

4.2. Magnetic resonance imaging protocols by domestic institutions

MRI protocols acquired for GKRS treatment planning at six domestic medical institutions were comparatively analyzed after being categorized into tumor, vascular, and nerve protocols. The MRI systems used across the six institutions were manufactured by GE, Siemens, and Philips. Imaging was performed using systems with

Table 4. Recommendations for guidelines in ISRS, German Taskforce, ESTRO-EANO.

Reference	Target scope and primary objectives	Recommendations	Resolution and key scan parameters
ISRS technical guidelines	Target: Small brain metastases (≤1 cm in diameter) and intracranial SRS Objective: Technical standardization and optimization of targeting accuracy	• 3D T1WI: Gradient echo (GRE), magnetization prepared rapid acquisition gradient echo (MPRAGE), brain volume imaging (BRAVO), fast low angle shot (FLASH), fast field echo (FFE) or spin echo (SE), sampling perfection with application optimized contrasts using different flip angle evolution (SPACE)	• Slice thickness: Fine-cut MR scans acquired ≤1.5 mm slice thickness • Contrast: Delayed post contrast imaging recommended • Scan timing: Delay after contrast agent administration • MRI-SRS interval: ≤7 days
German Taskforce (DIN 6864-1)	Target: Cranial SRT MRI Simulation Objective: Physical accuracy standardization according to German national standards (DIN)	• High resolution CE-T1WI as the main sequence for target delineation • Additional high resolution CISS, FIESTA or 3D T2WI FSE/TSE for target related cranial nerve target	• Patient position: Positioned as close as possible to the isocenter • Bandwidth: ≥ 440 Hz (to minimize chemical shift artifacts)
ESTRO-EANO	Target: Glioblastoma brain tumors requiring radiotherapy planning Objective: To standardize target delineation and radiotherapy planning details, including imaging, planning techniques, and fractionation.	• 3D CE-T1WI • T2WI/FLAIR	• Pre RT MRI acquired within ≤2 weeks before radiotherapy initiation • MRI acquisition preferably in treatment position • Planning CT with MRI co-registration/ fusion is recommended • Consistency between diagnostic and planning MRI recommended

magnetic field strengths of 1.5 T and 3.0 T, and considerable variability in hardware environments was observed among institutions, including coil channel ranging from 1 to 48 and differences in whether frame-based or frameless techniques were used. Accordingly, inter-institutional differences were identified in both the types of images acquired and the parameter settings applied.

Tables 5(a) and 5(b) present the detailed configurations of the GKRS planning MRI protocols for tumors at Hospitals A, B, and C, and Hospitals D, E, and F, respectively. In tumor protocols, depending on the institution and lesion type, tumor imaging for GKRS included not only CE-T1WI but also additional sequences such as T2WI, T1WI, CE-FLAIR, PD, CISS, contrast enhanced driven equilibrium (CE-DRIVE), contrast enhanced black blood imaging (CE-BB), and contrast enhanced spoiled gradient recalled echo (CE-SPGR). For T1WI and CE-T1WI, Institution A, under a 3.0 T environment, used

Table 5. (a) Imaging parameters of tumor at hospitals A, B, and C.

Hospital, MRI equipment (Frame or frameless / Coil / Position)	Protocols	Bandwidth	Acquisition matrix, phase encoding	Pulse sequence (Slice thickness)	TR, TE (msec)	Number of excitations	Flip angle (o)
A hospital, GE Healthcare SIGNA architect 3.0 T (Frameless / 48 channel head coil / HFS)	T2WI	122	256 × 256, Row	2D FSE (3mm)	4300, 90	1	142
	T1WI	244	320 × 260, Row	T1 IR (3 mm)	2340, 20	2	110
	CE-T1WI (Coronal)	122	256 × 256, Row	3D MPRAGE (1mm)	2330, 3	0.8	8
	CE-T1WI (Axial)			3D MPRAGE (3 mm)	2100, 3	1	8
	CISS	244	356 × 356, Row	3D CISS (1 mm)	5.6, 2.2		70
	CE-FLAIR		260 × 260, Row	3D FLAIR (2 mm)	10000, 100	1.7	160
B hospital, GE Healthcare SIGNA Premier 3.0 T (Frameless / 48 channel head coil / HFS)	T2WI	195	332 × 224, Row	2D FSE (1 mm)	8400, 100	1	140
	T1WI	140	280 × 280, Row	3D MPRAGE (1 mm)	2500, 3	0.8	8
	CE-T1WI						
	CE-FLAIR	245	230 × 230, Row	3D FLAIR FS (1 mm)	5000, 90	1	90
B hospital, Philips Intra Achiva 3.0 T (Frameless / 8 channel head coil / HFS)	T2WI	400	232 × 216, Row	2D TSE (1 mm)	3500, 100	1	90
	T1WI	430	275 × 275, Row	3D TFE (1 mm)	5, 2.5	1	8
	CE-T1WI					2	
	CE-FLAIR	280	220 × 165, Row	IR-TSE (1 mm)	10000, 120	1	90
C hospital, Philips Achieva 1.5 T (Frame or frameless / TR coil (Frame), 8 channel head coil (Frameless) / HFS)	CE-T1WI (Benign / Meta)	217	256 × 256, Row	3D FFE (3 mm) / 3D FFE (2 mm)	25, 5	1	30
	CE-T2WI (Benign / meta)	219		2D SE (2 mm)	7498, 80 / 14996, 80	2	90
	CE-DRIVE (Benign)	285.5		3D SE (1 mm)	1500, 160	1	90
	CE-T1WI delay (Meta)	217		3D FFE (3 mm)	25, 5	1	30
C hospital, Philips Ingenia CX 3.0 T (Frameless / 32 channel head coil / HFS)	PD (Benign)	345.5	304 × 304, Row	3D FSE (0.6 mm)	2000, 31	1	90
	T2WI (Benign)	1282.7	256 × 256, Row	2D FSE (2 mm)	4682, 80		
	CE-T1WI (Benign)	1251.9		3D FFE (3 mm)	6, 5		10
	CE-BB (Meta)	793.9	256 × 256, Column	3D FSE (1 mm)	500, 29		90
	CE-T2WI (Meta)	1282.7	256 × 256, Row	2D FSE (2 mm)	9364, 80		
	CE-T1WI delay (Meta)	1251.9		3D FFE (3 mm)	6, 5		10
C hospital, GE healthcare Discovery 3.0 T (Frameless / 32 channel head coil / HFS)	CE-SPGR	31.25	256 × 256, Row	3D VASC SPGR (0.6 mm)	6, 2	1	14

Table 5. (b) Imaging parameters of tumor at hospitals D, E, and F.

Hospital, MRI equipment (Frame or frameless / Coil / Position)	Protocols	Bandwidth	Acquisition matrix, phase encoding	Pulse sequence (Slice thickness)	TR, TE (msec)	Number of excitations	Flip angle (o)
D hospital, Philips Ingenia Ambition X 1.5 T (G-frame / 1 channel coil / HFS)	T2WI	218	320 × 320, Row	2D SE (2 mm)	8310, 80	2	90
	CE-T1WI (Axial)	145	512 × 512, Row	3D GRE (1.5 mm)	11, 5	1	8
	CE-T1WI (Coronal)						
	CISS	326		3D bFFE (1 mm)	7.5, 3.7	2	50
D hospital, Siemens magnetom VIDA 3.0 T (Frameless / Head and neck 20 channel coil / HFS)	T2WI	223	400 × 400, Row	2D SE (2 mm)	5500, 80	1	150
	CE-T1WI (Axial)	257	512 × 512, Row	3D MPRAGE (1.5 mm)	1400, 3		8
	CE-T1WI (Coronal)	180		3D VIBE (1.5 mm)	8, 3		9
E hospital, GE Healthcare SIGNA Explorer Infinity 1.5 T (G-frame / 1 channel head coil / HFS)	CE-T1WI	35.71	512 × 256, Difficulty in verification	3D BRAVO (2 mm)	10.8, 4.9	Difficulty in verification	
	T2WI	90.91		2D FSE (2 mm)	7480, 110		
				3D FRFSE-XL (3 mm)	2000, 120		
F hospital, GE Healthcare SIGNA 3.0 T (G-frame / 1 channel head coil / HFS)	T2WI	50	260 × 260, Row	2D FSE (2 mm)	12528, 120	1.5	100
	CE-T1WI	15.63	228 × 228, Row	3D BRAVO (2 mm)	11.6, 4.8	1	10

T1WI IR (3 mm) and 3D MPRAGE (1~3 mm), with an acquisition matrix of 256 × 256 to 320 × 260, BW of 122~244 Hz, TR of 2100~2340 msec, TE of 3~20 msec, NEX of 0.8~2, and FA of 8~110°. Institution B, using 3.0 T systems, acquired 1 mm 3D MPRAGE and turbo field echo (TFE), with an acquisition matrix of 275 × 275 to 280 × 280, BW of 140~430 Hz, and FA of 8°. Institution C, at 3.0 T, acquired 3D FFE (3 mm, BW 1251.9 Hz, FA 10°) and 3D VASC SPGR (0.6 mm, BW 31.25 Hz, FA 14°), whereas at 1.5 T it applied 2~3 mm 3D FFE (BW 217 Hz, FA 30°). Institution D (1.5 T and 3.0 T) used 1.5 mm 3D GRE, MPRAGE, and volumetric interpolated breath-hold examination (VIBE), with an acquisition matrix of 512 × 512, BW of 145~257 Hz, and FA of 8~9°. Institutions E and F (G-frame, 1-channel) used 2 mm 3D BRAVO, with BW of 15.63~35.71 Hz, an acquisition matrix of 228 × 228 to 512 × 256, TR of 10.8~11.6 msec, TE of 4.8~4.9 msec, and FA of 10°.

For T2WI and CE-T2WI, Institution B acquired 1 mm 2D fast spin echo (FSE) and turbo spin echo (TSE) images (BW 195~400 Hz, TR 3500~8400 msec, TE 100 msec). Institutions A and C (3.0 T) applied 2~3 mm 2D FSE (BW 122~1282.7 Hz), whereas Institution C (1.5 T) and Institution D applied 2 mm 2D spin echo (SE) (BW 218~223 Hz, TR 5500~8310 msec, TE 80 msec). Institution C additionally acquired 2 mm CE-T2WI (2D SE and 2D FSE). Institution E acquired 2 mm 2D FSE as well as an additional 3 mm 3D fast relaxation fast spin echo–extra length (FRFSE-XL) sequence (TR 2000 msec, TE 120 msec), whereas Institution F used 2 mm 2D FSE with BW 50 Hz, TR 12528 msec, TE 120 msec, NEX 1.5, and FA 100°.

For CE-FLAIR, PD, and other 3D sequences, Institution A acquired 2 mm 3D FLAIR (BW 244 Hz, acquisition matrix 260 × 260, TR 10000 msec, TE 100 msec, NEX 1.7, FA 160°) and 1 mm 3D CISS (BW 244 Hz, FA 70°). Institution B acquired 1 mm CE-FLAIR and IR~TSE (BW 245~280 Hz, TR 5000~10000 msec, TE 90~120 msec, FA 90°). Institution C (3.0 T) included 0.6 mm 3D FSE PD (BW 345.5 Hz, TR 2000 msec, TE 31 msec, FA 90°) and 1 mm 3D FSE CE-BB (BW 793.9 Hz, TR 500 msec, TE 29 msec, FA 90°), whereas at 1.5 T it acquired 1 mm 3D SE CE-DRIVE (BW 285.5 Hz, TR 1500 msec, TE 160 msec, FA 90°).

Tables 6(a) and 6(b) present the detailed configurations of the GKRS planning MRI protocols for vascular diseases at Hospitals A, B, and C, and Hospitals D, E, and F, respectively. Vascular imaging for GKRS was centered on 3D TOF and CE-TOF, with additional T1WI, CE-T1WI, T2WI, and CE-FLAIR sequences acquired as needed. For TOF and CE-TOF, Institution A (3.0 T) applied 1 mm 3D TOF with an acquisition matrix of 640 × 320, BW of 97 Hz, TR of 13 msec, TE of 3 msec, NEX of 0.8, and FA of 18°. Institution B (3.0 T) used 0.5~0.8

Table 6. (a) Imaging parameters of vascular at hospitals A, B, and C.

Hospital, MRI equipment (Frame or frameless / Coil / Position)	Protocols	Bandwidth	Acquisition matrix, phase encoding	Pulse sequence (Slice thickness)	TR, TE (msec)	Number of excitations	Flip angle (o)
A hospital, GE Healthcare SIGNA architect 3.0 T (Frameless / 21 channel head and neck coil / HFS)	T2WI	122	256 × 256, Row	2D FSE (3 mm)	4000, 80	1	142
	T1WI	244	256 × 256, Row	2D SE (3 mm)	550, 80	1	90
	CE-T1WI (Coronal)	122	256 × 256, Row	3D MPRAGE (1 mm)	2100, 30	1	8
	CE-T1WI	122	256 × 256, Row	3D MPRAGE (3 mm)	2330, 3	0.8	8
	CE-TOF	97	640 × 320, Row	3D TOF (1 mm)	13, 3	0.8	18
	CE-FLAIR	97	260 × 260, Row	3D FLAIR (2 mm)	10000, 100	1.7	160
B hospital, GE Healthcare SIGNA Premier 3.0 T (Frameless / 48 channel head coil / HFS)	T2WI	195	332 × 224, Row	2D FSE (1 mm)	4500, 100	1	140
	TOF	140	416 × 256, Row	3D TOF MRA (0.5 mm)	20, 3	0.85	15
	CE-TOF						
	CE-T1WI		280 × 280, Row	3D MPRAGE (1 mm)	2500, 3	1	90
B hospital, Philips Intra Achiva 3.0 T (Frameless / Multi head coil / HFS)	T2WI	400	256 × 256, Row	2D TSE (1 mm)	4500, 100	1	140
	TOF	170	512 × 256, Row	3D csTOF (0.8 mm)	20, 3	0.85	15
	CE-TOF						
	CE-T1WI	430	275 × 275, Row	3D TFE (1 mm)	2500, 3	1	8
C hospital, Philips Achieva 1.5 T (Frame or frameless / TR coil (Frame), 8 channel head coil (Frameless) / HFS)	TOF	108.8	320 × 256, Row	3D TOF (2 mm)	27, 7	1	25
	T2WI	219	256 × 256, Row	2D SE (2 mm)	5832, 80	2	90
	CE-T1WI	217		3D FFE (3 mm)	25, 5	1	30
C hospital, GE healthcare Discovery 3.0 T (Frameless / 32 channel head coil / HFS)	TOF	41.67	416 × 288, Row	3D VASC TOF (1.2 mm)	23, 4	1.5	18

Table 6. (b) Imaging parameters of vascular at hospitals D, E, and F.

Hospital, MRI equipment (Frame or frameless / Coil / Position)	Protocols	Bandwidth	Acquisition matrix, phase encoding	Pulse sequence (Slice thickness)	TR, TE (msec)	Number of excitations	Flip angle (o)
D hospital, Philips Ingenia Ambition X 1.5 T (G-frame / 1 channel coil / HFS)	T2WI	218	320 × 320, Row	2D SE (2 mm)	8310, 80	1	90
	CE-T1WI	145	512 × 512, Row	3D GRE (1.5 mm)	11, 5		8
D hospital, Siemens magnetom VIDA 3.0 T (Frameless / Head and neck 20 channel coil / HFS)	T2WI	223	400 × 400, Row	2D SE (2 mm)	5500, 80	1	150
	CE-T1WI	257	512 × 512, Row	3D MPRAGE (1.5 mm)	1400, 3		8
	CE-TOF	157	352 × 340, Row	3D TOF MRA (0.6 mm)	22, 3.7		15
E hospital, GE Healthcare SIGNA Explorer Infinity 1.5 T (G-frame / 1 channel head and neck coil / HFS)	T1WI	35.71	512 × 256, Difficulty in verification	3D BRAVO (2 mm)	10.8, 4.9	Difficulty in verification	
	CE-T1WI	65.71					
	T2WI	90.91		2D FSE (2 mm)	7480, 110		
F hospital, GE Healthcare SIGNA 3.0 T (G-frame / 1 channel head coil / HFS)	T2WI	50	260 × 260, Row	2D FSE (2 mm)	12528, 120	1.5	100
	TOF	25		3D TOF MRA (2 mm)	Min, 3.4	0.85	18
	CE-TOF						

mm 3D TOF and compressed sense TOF (csTOF), with an acquisition matrix of 416 × 256 to 512 × 256, BW of 140~170 Hz, TR of 20 msec, TE of 3 msec, NEX of 0.85, and FA of 15°. Institution C (3.0 T) acquired 1.2 mm 3D VASC TOF (acquisition matrix 416 × 288, BW 41.67 Hz, NEX 1.5, FA 18°), whereas at 1.5 T it applied 2 mm 3D TOF (BW 108.8 Hz). Institution D (3.0 T) acquired 0.6 mm 3D TOF (acquisition matrix 352 × 340, BW 157 Hz, TR 22 msec, TE 3.7 msec, FA 15°). Institution F used 2 mm 3D TOF with BW 25 Hz, minimum TR, TE 3.4 msec, NEX 0.85, and FA 18°.

For T1WI and CE-T1WI within vascular protocols, Institution B acquired 1 mm 3D MPRAGE and TFE. Institution A acquired 3 mm 2D SE (T1WI) and 1~3 mm 3D MPRAGE (CE-T1WI). Institution D applied 1.5 mm 3D GRE and MPRAGE, whereas Institution C (1.5 T) acquired 3 mm 3D FFE. Institution E used 2 mm 3D BRAVO for T1WI and CE-T1WI with BW of 65.71 Hz.

For T2WI and CE-FLAIR, Institution B applied 1 mm 2D FSE and TSE (BW 195~400 Hz). Institution A acquired 3 mm 2D FSE (BW 122 Hz, TR 4000 msec, TE 80 msec) together with 2 mm 3D FLAIR (BW 97 Hz, TR 10000 msec, TE 100 msec). Institutions C (1.5 T) and D applied 2 mm 2D SE (BW 218~223 Hz), whereas Institutions E and F acquired 2 mm 2D FSE (BW 50~90.91 Hz).

Tables 7(a) and 7(b) present the detailed configurations of the GKRS planning MRI protocols for cranial nerves at Hospitals A, B, and C, and Hospitals D, E, and F, respectively. These nerve protocols predominantly utilized specialized 3D sequences such as CISS, FIESTA, DRIVE, volume isotropic turbo spin echo acquisition (VISTA), CUBE, and PD, whereas T1WI, CE-T1WI, T2WI, and TOF were acquired as supplementary examinations. For CISS, FIESTA, VISTA, CUBE, PD, and DRIVE, Institution A (1.5 T) acquired 1 mm 3D CISS (acquisition matrix

Table 7. (a) Imaging parameters of nerve at hospitals A, B, and C.

Hospital, MRI equipment (Frame or frameless / Coil / Position)	Protocols	Bandwidth	Acquisition matrix, phase encoding	Pulse sequence (Slice thickness)	TR, TE (msec)	Number of excitations	Flip angle (o)
A hospital, Siemens magnetom sola 1.5 T (G-frame / TxRx CP head coil / HFS)	T1WI	130	256 × 256, Row	2D SE (2 mm)	500, 9.5	1	90
	T2WI			2D TSE (2 mm)	6100, 84	2	170
	CE-T1WI (Coronal)			3D MPRAGE (2 mm)	1290, 3.5	1	15
	CE-T1WI (Axial)			3D MPRAGE (1 mm)	2000, 3.5		
	CISS	352	352 × 380, Column	3D CISS (1 mm)	6.8, 3.4		80
B hospital, GE Healthcare SIGNA Premier 3.0 T (Frameless / 48 channel head coil / HFS)	T2WI	195	332 × 224, Row	2D FSE (1 mm)	8400, 100	1	140
	T1WI	140	280 × 280, Row	3D MPRAGE (1 mm)	2500, 3	0.8	8
	CE-T1WI						
	Cube	160	300 × 300, Row	3D T2 CUBE Heavily (1.5 mm)	1800, 280	1	90
	PD		320 × 320, Row	3D PD CUBE (0.7 mm)	1300, 30	0.82	
B hospital, Philips Intra Achiva 3.0 T (Frameless / 8 channel neurovascular coil / HFS)	T2WI	400	232 × 216, Row	2D TSE (1 mm)	3500, 100	1	90
	T1WI	430	275 × 275, Row	3D TFE (1 mm)	5, 2.5	1	8
	CE-T1WI					2	
	Vista	300	345 × 345, Row	3D T2 VISTA (0.75 mm)	2000, 300	1	90
	PD	500	228 × 228, Row	3D PD (0.36 mm)	2000, 30		
C hospital, Philips Achieva 1.5 T (Frame or frameless / TR coil (Frame), 8 channel head coil (Frameless) / HFS)	TOF	108.8	320 × 256, Row	3D TOF (2 mm)	27, 7	1	25
	DRIVE	285.5	256 × 256, Row	3D SE (1 mm)	1500, 160		90
	CE-T1WI	217	256 × 256, Row	3D FFE (2 mm)	25, 5		30
C hospital, Philips Ingenia CX 3.0 T (Frameless / 32 channel head coil / HFS)	PD	363.4	208 × 208, Row	3D FSE (1 mm)	2000, 28	1	90
	TOF	173.6	640 × 333, Row	3D TOF (1 mm)	20, 3		18
	CE-T1WI	1251.9	256 × 256, Row	3D FFE (2 mm)	6, 5		10

Table 7. (b).Imaging parameters of nerve at hospitals D, E, and F.

Hospital, MRI equipment (Frame or frameless / Coil / Position)	Protocols	Bandwidth	Acquisition matrix, phase encoding	Pulse sequence (Slice thickness)	TR, TE (msec)	Number of excitations	Flip angle (o)
D hospital, Philips Ingenia CX 3.0 T (Vantage frame / Head TR 1 channel coil / HFS)	CISS	428	512 × 512, Row	3D bTFE GR (0.6 mm)	6, 3	2	50
	T1WI	388		3D T1 GRE (1.5 mm)	6.5, 3.4		8
E hospital, GE Healthcare SIGNA Explorer Infinity 1.5 T (G-frame / 1 channel head and neck coil / HFS)	T1WI	35.71	512 × 256, Difficulty in verification	3D BRAVO (2 mm)	10.8, 4.9	Difficulty in verification	
	T2WI	90.91		2D FSE (2 mm)	7480, 110		
	FIESTA	62.50		3D FIESTA (1 mm)	6.9, min.		
F hospital, GE Healthcare SIGNA 3.0 T (G-frame / 1 channel head coil / HFS)	T2WI	50	260 × 260	2D FSE (2 mm)	12528, 120	1.5	100
	T1WI	15.63	228 × 228	3D BRAVO (2 mm)	11.6, 4.8	1	10
	CISS	62.5	260 × 260	3D CISS (0.5 mm)	529, 13		-

352 × 380, BW 352 Hz, TR 6.8 msec, TE 3.4 msec, FA 80°). Institution B, using 3.0 T systems, acquired 1.5 mm 3D T2 CUBE (BW 160 Hz, TR 1800 msec, TE 280 msec, FA 90°), 0.7 mm 3D PD CUBE (TR 1300 msec, TE 30 msec), 0.75 mm 3D T2 VISTA (BW 300 Hz, TR 2000 msec, TE 300 msec, FA 90°), and 0.36 mm 3D PD (BW 500 Hz, TR 2000 msec, TE 30 msec). Institution C (1.5 T) acquired 1 mm 3D SE DRIVE (BW 285.5 Hz, TR 1500 msec, TE 160 msec, FA 90°), whereas at 3.0 T it acquired 1 mm 3D FSE PD (BW 363.4 Hz, TR 2000 msec, TE 28 msec, FA 90°). Institution D (3.0 T) acquired 0.6 mm 3D balanced turbo field echo (bTFE), CISS (acquisition matrix 512 × 512, BW 428 Hz, TR 6 msec, TE 3 msec, NEX 2, FA 50°). Institution E applied 1 mm 3D FIESTA (BW 62.5 Hz, TR 6.9 msec, minimum TE), whereas Institution F acquired 0.5 mm 3D CISS (acquisition matrix 260 × 260, BW 62.5 Hz, TR 529 msec, TE 13 msec).

For T1WI and CE-T1WI, Institution A acquired 2 mm 2D SE (T1WI) and 1~2 mm 3D MPRAGE (CE-T1WI). Institution B acquired 1 mm 3D MPRAGE and 3D TFE. Institution C applied 2 mm 3D FFE (BW 217~1251.9 Hz), whereas Institution D acquired 1.5 mm 3D T1 GRE (BW 388 Hz, FA 8°). Institutions E and F applied 2 mm 3D BRAVO (BW 15.63~35.71 Hz) for T1WI acquisition.

For T2WI and TOF, Institution A acquired 2 mm 2D TSE (TR 6100 msec, TE 84 msec, NEX 2, FA 170°). Institution B applied 1 mm 2D FSE and 2D TSE (BW 195~400 Hz). Institutions E and F acquired 2 mm 2D FSE. Institution C included 1~2 mm 3D TOF (BW 108.8~173.6 Hz, TR 20~27 msec, TE 3~7 msec) within the nerve protocol.

5. Discussions

Diseases arising in the brain include tumors, vascular disorders, and functional diseases, and active treatment is required because these conditions can adversely affect not only physical function but also emotional well-being [27]. The establishment of a treatment strategy involves comprehensive consideration of the patient's condition, age, severity of symptoms, and type of disease, and imaging evaluation is fundamentally required before determining the optimal therapeutic approach. Each disease has its own inherent characteristics, and imaging studies can visually depict these distinctive features and patterns, thereby assisting in the formulation of the most appropriate treatment strategy based on an accurate diagnosis [5, 6]. The importance of imaging technology in disease diagnosis and treatment continues to grow, and in particular, radiosurgical procedures such as GKRS require image-based treatment planning; therefore, a thorough understanding of imaging techniques capable of depicting lesions with high spatial resolution is essential [6, 14].

MRI is the imaging modality that plays the most important role in establishing a radiosurgical treatment plan for GKRS. Because GKRS controls the lesion by prescribing a high radiation dose to the boundary between diseased tissue and normal tissue, accurate delineation of this interface is of paramount importance. MRI provides high resolution visualization of these tissue boundaries, thereby creating an imaging environment that enables precise prescription of high radiation doses in GKRS [6, 7, 24–27].

As of 2022, a total of 1,897 MRI systems had been installed in domestic medical institutions, indicating

broad accessibility to the clinical use of MRI [32]. Although these systems are managed according to consistent institutional regulations, in actual clinical practice the specifications of MRI equipment, imaging techniques, and detailed acquisition parameters inevitably vary across institutions. Even for the same disease, differences in image quality may arise among institutions, which can lead to inaccuracies in GKRS treatment planning. Although related guidelines have been proposed by international organizations, there are practical limitations to directly applying them to the domestic medical system, reimbursement standards, and multicenter data compatibility in Korea [14–20]. Accordingly, as part of an effort to improve the precision of GKRS, the present study investigated and comparatively analyzed MRI acquisition conditions across multiple institutions, with the aim of providing an academic foundation for the future development of standardized MRI protocol recommendations tailored to domestic clinical practice.

First, among the recommendations issued by international organizations, the major points of emphasis were the control of image distortion and the application of highly precise imaging to SRS [14–20]. As a key strategy for achieving this, the use of multimodality image fusion was suggested to be useful, and, based on currently available pulse sequences, CE-T1WI was proposed as a valuable MRI dataset for targeting contrast-enhancing lesions. When the target is located close to organs at risk, the usefulness of additional high resolution techniques such as CISS and FIESTA was also highlighted. In particular, the importance of slice thickness was repeatedly emphasized [14, 15, 18]. Slice thickness is closely related to the partial volume effect, and, in general, an increase in slice thickness leads to an increase in the partial volume effect [33]. Increased partial volume effects reduce the resolution of the boundary between diseased tissue and normal tissue, and GKRS is characterized by the delivery of very high radiation doses in a single fraction, or in a small number of fractions, precisely at the interface between adjacent tissues. When this treatment characteristic is combined with an increased partial volume effect, the risk of radiation-related complications may increase. Therefore, the emphasis placed on slice thickness as a physical parameter, along with the recommendation of specific thickness values, appears to reflect an effort to enable meticulous disease targeting.

RANO 2.0 recommended MRI acquisition compatible with the BTIP. For 3D T1WI, it emphasized the need for high resolution MRI data to allow accurate volumetric assessment and, when feasible, recommended parameter matching between pre- and post-contrast 3D T1WI acquisitions. In addition, the usefulness of sequences such as T2WI, FLAIR, and DWI was also confirmed [16, 17]. In particular, for 2D sequences, image acquisition with no slice gap whenever possible was recommended in order to minimize error [17]. This measure is intended to prevent small lesions from being missed or distorted. Another notable point was the explicit recommendation of delayed post-contrast imaging. This appears to represent a minimal strategy to overcome inter-institutional differences in workflow and slice-thickness variation, with the aim of enabling more consistent assessment of treatment response in radiotherapy and radiosurgery.

Other SRS-related guidelines also showed a common emphasis on securing physical precision and clinical consistency through optimization of sequence composition and imaging parameters [18–20]. The ISRS technical guidelines recommended thin slice thickness for accurate localization of small brain metastases and indicated that reducing slice thickness may improve localization accuracy [18]. For the detection of contrast-enhancing lesions, the guidelines recommended image acquisition after a delay following contrast administration and also proposed maintaining an appropriate interval between MRI and the actual SRS procedure [18]. The German Taskforce DIN 6864-1 recommended the use of high resolution CE-T1WI for MRI simulation in cranial stereotactic radiotherapy and further advised that, for lesions adjacent to cranial nerves, the additional acquisition of high resolution 3D-based sequences such as CISS or FIESTA is particularly useful [19]. In addition, the guideline stated that the region of interest should be positioned as close as possible to the magnet and gradient isocenter in order to reduce geometric distortion, and recommended that the pixel BW be set to at least 440 Hz to minimize distortions caused by B0 inhomogeneity and chemical shift [19]. The ESTRO-EANO guideline recommended that, in order to improve the consistency and accuracy of radiotherapy planning, pre-treatment MRI should be obtained within 2 weeks before the start of radiotherapy, preferably in a position similar to the actual treatment position, and should be fused with CT simulation images [20]. These recommendations may be understood as measures intended to reduce temporal and technical variability between image acquisition and treatment planning, thereby improving the reproducibility of target delineation and treatment response assessment.

Based on these findings, the MRI-related parameters used at six domestic institutions were analyzed, and considerable variability was observed. Overall, despite the heterogeneity of their adopted MRI hardware environments, domestic institutions demonstrated a tendency to ensure

physical precision and consistency in clinical outcomes. When compared with international guidelines, this was largely achieved through the utilization of thin slice thicknesses and the application of MRI techniques tailored to the clinical characteristics of each disease to support precise targeting.

International recommendations advocate the use of thin slice thickness in order to minimize partial volume effects that may arise from thicker sections. In the present analysis, domestic institutions equipped with 3.0 T systems and multichannel coils in a frameless environment were found to apply thin slice thickness consistently in 3D CE-T1WI acquisition for tumor protocols. In vascular protocols as well, thin slice thickness was used for imaging techniques intended to delineate fine vascular structures, and cases were also identified in which ultra-high resolution acquisition matrices were proactively applied. This tendency was similarly maintained in nerve protocols. These configurations align with the technical elements emphasized in international guidelines for target localization and the evaluation of anatomical structures. However, since this study did not directly measure dose calculation errors, target localization accuracy, or treatment outcomes, it cannot be definitively concluded that these protocols improve such clinical results.

From a clinical perspective, domestic institutions were faithfully reflecting international recommendations by employing imaging techniques that extended beyond the minimum suggested requirements in order to maintain treatment efficacy at a consistent level. In the tumor protocol, one institution was using a delayed CE-T1WI technique, indicating that the recommendation for a post-contrast delay had been adapted to the domestic clinical setting to improve the detection rate of metastatic brain tumors and support more accurate targeting. The vascular protocol also incorporated techniques such as T2WI, TOF, and CE-TOF to delineate the complex architecture of the nidus. Notably, in the nerve protocol, most domestic institutions did not rely solely on conventional T2WI, but instead adopted specialized pulse sequence–based techniques such as CISS, FIESTA, and DRIVE. At the same time, the use of flip angles ranging from 50° to 90° to enhance contrast between neural structures and cerebrospinal fluid represents an example of highly advanced clinical application. However, this study did not directly evaluate whether these sequence configurations improve lesion detectability, the reproducibility of target delineation, or clinical outcomes.

The physical and clinical characteristics of domestic institutions performing MRI in a frame-based environment using 1.5 T or 3.0 T systems combined with a 1-channel coil showed somewhat different patterns from those observed in the previously described settings. When imaging is performed with a fixed stereotactic frame, the frame occupies substantial space, making the use of multichannel coils difficult; accordingly, MRI is generally performed using a 1-channel coil. Considering the transmit–receive efficiency of a 1-channel coil, the application of a thin slice thickness can adversely affect the signal to noise ratio (SNR), one of the key determinants of image quality. This, in turn, results in increased image noise and substantial difficulty in lesion detection. Therefore, the relatively greater slice thickness used in frame-based MRI compared with frameless imaging reflects a practical compromise made to secure adequate SNR while still considering international recommendations. In addition, when T1-weighted sequences were acquired in the tumor, vascular, and nerve protocols, pulse sequences such as GRE, FFE, and BRAVO were consistently used as the primary techniques. This suggests the application of a strategy intended to compensate for the lower SNR of the 1-channel coil within a relatively short acquisition time, while maintaining an acceptable slice thickness and ensuring stable T1 contrast for accurate targeting. From a clinical standpoint, as in frameless environments, these institutions were found to faithfully implement international recommendations by using a variety of imaging techniques to enhance treatment efficacy. Notably, in the nerve protocol, unlike the general pattern described above, even thinner slice thicknesses and specialized techniques such as FIESTA and CISS were applied, reflecting efforts within the domestic clinical environment to achieve the specific clinical objectives required for diagnosis and surgical planning in these disorders.

Conversely, with the exception of a few sequences, the BWs used in the participating domestic centers were frequently observed to be lower than the values recommended by international guidelines. These ranges varied depending on the MRI manufacturer, magnetic field strength, coil configuration, use of a stereotactic frame, and sequence characteristics. Generally, it is known that BW helps reduce distortions associated with magnetic field inhomogeneities and chemical shift, which necessitates a balance with the SNR [34]. However, because this study did not perform a direct quantitative evaluation of SNR, geometric distortion, or target localization accuracy, it cannot be determined whether the observed BW settings were the result of an intentional trade off considering these physical parameters [34-36].

In addition, several limitations were observed with respect to clinical consistency, including insufficient control of post-contrast delay time, mismatched T1WI

parameters before and after contrast administration, and limited use of auxiliary imaging techniques for edema assessment. Regarding post-contrast delay time, except for one institution that applied a delayed CE-T1WI technique for targeting metastatic brain tumors, no evidence of implementation of such an approach was identified at the other institutions. Furthermore, international recommendations emphasize the importance of matching pre- and post-contrast imaging parameters. Although there were some positive examples in which certain institutions attempted parameter matching by using the same MPRAGE (1 mm) and BRAVO (2 mm) sequences before and after contrast administration, most domestic protocols remained primarily focused on visual diagnosis of lesions. Similarly, auxiliary techniques such as FLAIR for edema assessment were found to be used only selectively at a limited number of institutions. The absence of consistent control of post-contrast timing, the mismatch of T1WI parameters before and after contrast administration, and the limited use of FLAIR may all be factors that hinder future standardization and inter-institutional comparability of multicenter clinical data for GKRS.

The comparative analysis of GKRS MRI protocols among domestic institutions revealed that all centers successfully reproduced physical parameters to secure the optimal image contrast necessary for precise targeting of tumor, vascular, and nerve structures. To achieve this, it was confirmed that each hospital adjusted the types of pulse sequences and the ranges of TR, TE, and FA. These optimizations were tailored to the specific environmental constraints and characteristics of each institution, heavily depending on their hardware specifications, such as the MRI model, coil channel configuration, and magnetic field strength. For acquisition of T2WI to evaluate peritumoral edema or anatomical structures in brain tumors, all institutions used 2D FSE, TSE, or SE techniques. To depict cerebrospinal fluid as high signal intensity and enhance tissue contrast, TR was set in the range of 3500~12528 msec, TE in the range of 80~120 msec, and FA was consistently applied between 90° and 170°, indicating an effort to maximize T2 relaxation effects. In vascular protocols, all institutions without exception used TOF imaging to take advantage of the inflow enhancement effect of blood flow, with TR set at 13~27 msec, TE at 3~7 msec, and FA at 15~25° to secure sufficient contrast. In the case of T1WI and nerve protocols, parameter differences were observed according to scanner manufacturer. For CE-T1WI acquisition in a 3.0 T frameless environment, MPRAGE was predominantly used, with TR values of 1400~2500 msec, TE values of 3~3.5 msec, and an FA of 8°. In contrast, frame-based MRI environments and some Philips systems used techniques such as BRAVO, FFE, and GRE, with TR values distributed between 6 and 25 msec, TE values between 2.5 and 5 msec, and FA values between 8° and 30°. These differences appear to result from differences in the mechanisms of the pulse sequences selected to achieve optimal T1 contrast depending on scanner specifications. In nerve protocols, when most institutions used CISS or FIESTA, TR ranged from 5.6 to 6.9 msec, TE from 2.2 to 3.4 msec, and FA from 50° to 80°. In contrast, one institution used FSE-based VISTA and CUBE pulse sequences, with TR values of 1800~2000 msec, TE values of 280~300 msec, and an FA of 90°, demonstrating a different approach to securing contrast.

The limitations of this study are as follows. First, there are inherent limitations regarding representativeness, as this was a preliminary multicenter study involving institutions available for participation rather than a randomized sampling of all GKRS centers in Korea. In particular, the small sample size of six participating institutions introduces the potential for selection bias. Additionally, further verification of the data collected from each institution was limited, and the selection of international recommendations used for comparison lacked a highly systematic process. Therefore, cautious interpretation is required when generalizing these findings to all GKRS facilities nationwide.

Second, this study was conducted as a multicenter survey intended to investigate the current status of MRI protocols actively used in domestic GKRS facilities and to propose directions for standardization. From a technical perspective, fundamental differences exist in sequence nomenclature and implementation methods among MRI manufacturers. Consequently, even nominally identical parameters may not yield equivalent imaging characteristics across different vendors. Therefore, directly comparing or verifying image quality or clinical performance fell outside the scope of this study. Specifically, evaluating image quality and dosimetric verification requires a comprehensive analysis of the overall clinical data of actual GKRS patients. Such data involve institutional clinical imaging and treatment planning data, which are inextricably linked to each center's imaging equipment, treatment planning systems, and data management frameworks. Furthermore, practical limitations prevented the collection and direct comparison of data across multiple centers under a unified standard, primarily due to strict patient privacy protections, institutional research ethics, and data-sharing policies. As a result, we could not directly assess these elements. Thus, the MRI protocols proposed in this study should be interpreted not as

guidelines demonstrating the superiority of specific imaging parameters, but rather as practical recommendations formulated by synthesizing existing literature and the real-world clinical experiences of major domestic Gamma Knife centers. Finally, it should be explicitly stated that this proposed direction was not established through a formal expert consensus process.

Third, as a descriptive survey study comparing the parameter settings of GKRS planning MRI protocols across institutions, this research confirmed that a substantial number of centers utilize BWs lower than international recommendations. However, direct measurements of SNR, geometric distortion, image quality, target delineation reproducibility, and clinical outcomes in relation to variations in BW were not performed. Consequently, the appropriateness of the lower BW settings observed herein, or the causal relationship between BW and image quality, cannot be directly determined. In the future, prospective multicenter collaborative studies utilizing standardized patient imaging and treatment planning data are necessary. Such studies should comprehensively verify image quality, geometric accuracy, target delineation reproducibility, clinical validity, and the actual impact of BW on GKRS. Furthermore, based on these collective efforts, the formation of a systematic expert consensus body should follow to establish formal practical guidelines.

Fourth, the lack of clinical protocol consistency across multiple centers, as identified by the survey results, constitutes another practical limitation inherent in this study. In a substantial number of institutions, the management of post-contrast delay times—which is crucial for the precise targeting of metastatic lesions—was suboptimal. Furthermore, we identified potential parameter mismatches between pre- and post-contrast T1WI, which are required for accurate volumetric comparisons, and found that the utilization of FLAIR sequences, useful for evaluating edema, was also limited. These findings indicate that the current landscape of domestic multicenter protocols does not fully satisfy international recommendations in terms of clinical workflow. This strongly suggests that supplementing detailed practical guidelines is essential to improve inter-institutional consistency in the future.

6. Conclusion

In this study, MRI protocols used for GKRS planning at six domestic institutions were comparatively analyzed after being categorized into tumor, vascular, and nerve protocols, and these findings were compared with international guidelines in order to propose a direction for standardization tailored to the domestic clinical setting. A comparative analysis against international guidelines using pre-defined indicators revealed that domestic institutions demonstrated notable efforts to prioritize the reproducibility of target delineation. This was achieved by securing geometric precision through the application of thin slice thicknesses, the utilization of disease specific sequences, and the acquisition of high resolution images. However, overall, there were clear limitations in concluding that these protocols fully satisfy international recommendations. Specifically, inter-institutional variations in compliance and certain shortcomings in protocol configurations and parameter settings were identified—particularly regarding the use of low BWs, management of post-contrast delay times, and the limited utilization of auxiliary sequences such as FLAIR. These variations depended heavily on the MRI manufacturer, magnetic field strength, coil channel configuration, and the use of frame-based or frameless systems. Furthermore, because this study did not directly verify actual physical precision or target localization accuracy, it cannot be definitively concluded that these protocol settings are technically flawless or that they guarantee improved clinical outcomes.

Accordingly, standardization of MRI for GKRS in Korea should be established not on the basis of uniform fixed values, but rather in the form of recommendations that reflect the type of MRI system, the associated hardware environment, and the intended clinical purpose. In settings utilizing 3.0 T frameless systems and multi-channel coils, thin-slice 3D CE-T1WI and high resolution isotropic acquisition can be recommended. In contrast, for frame-based single-channel coil environments, slice thickness and BW settings may be configured differently from those in frameless multi-channel setups due to inherent constraints in equipment and coil configurations. Therefore, it is necessary for future standardization guidelines to separately verify and propose applicable parameter ranges tailored to each specific hardware environment. Vendor-specific 3D T1 sequences, such as MPRAGE, BRAVO, FFE, and GRE, should be grouped and presented as sequences serving the same purpose. For the nerve protocol, it appears desirable to allow high resolution specialized sequences specific to each system, such as CISS, FIESTA, DRIVE, VISTA, and CUBE, as alternative options. For the vascular protocol, standardized criteria may be developed on the basis of high resolution image acquisition using TOF and CE-TOF. In the tumor protocol, further standardization appears necessary with respect to post-contrast delay time, parameter matching before and after contrast administration, and the use of FLAIR.

In conclusion, this direction of standardization would allow newly established centers or institutions replacing

MRI equipment to more easily re-establish GKRS planning MRI settings according to the characteristics of their systems. It is also expected to contribute to improving the consistency of image quality and the reliability of data in multicenter GKRS planning MRI across Korea. Furthermore, the present study may serve as foundational data for the development of a Korean guideline for MRI standardization in GKRS.

References

[1] European Society of Radiology, Insights Imaging **6**, 141 (2015).

[2] C. Coolens, M. N. Gwilliam, P. Alcaide-Leon, I. M. de Freitas Faria, and F. Y. de Moraes, Cancers **13**, 2557 (2021).

[3] J. Huang, Y. Xiang, S. Gan, L. Wu, J. Yan, D. Ye, and J. Zhang, Discov. Oncol. **16**, 1625 (2025).

[4] J. D. Shur, S. J. Doran, S. Kumar, D. ap Dafydd, K. Downey, J. P. B. O'Connor, N. Papanikolaou, C. Messiou, D. M. Koh, and M. R. Orton, RadioGraphics **41**, 1717 (2021).

[5] J. Regis, C. Tuleasca, N. Resseguier, R. Carron, A. Donnet, J. Gaudart, and M. Levivier, J. Neurosurg. **124**, 1079 (2016).

[6] J. Jagannathan, C. P. Yen, D. K. Ray, D. Schlesinger, R. J. Oskouian, N. Pouratian, M. E. Shaffrey, J. Larner, and J. P. Sheehan, J. Neurosurg. **111**, 431 (2009).

[7] Y. Huang, E. Liang, E. M. Schaff, B. Zhao, K. C. Snyder, I. J. Chetty, M. M. Shah, and S. M. Siddiqui, Front. Oncol. **13**, 1090582 (2023).

[8] C. M. Pirkl, L. Nunez-Gonzalez, F. Kofler, S. Endt, L. Grundl, M. Golbabaee, P. A. Gómez, M. Cencini, G. Buonincontri, R. F. Schulte, M. Smits, B. Wiestler, B. H. Menze, M. I. Menzel, and J. A. Hernandez-Tamames, Neuroradiology **63**, 1831 (2021).

[9] E. H. Herskovits, R. Itoh, and E. R. Melhem, AJR Am. J. Roentgenol. **176**, 1313 (2001).

[10] G. S. Tandel, A. Tiwari, O. G. Kakde, N. Gupta, L. Saba, and J. S. Suri, Diagnostics **13**, 481 (2023).

[11] C. K. Glide-Hurst, E. S. Paulson, K. McGee, N. Tyagi, Y. Hu, J. Balter, and J. Bayouth, Med. Phys. **48**, e636 (2021).

[12] S. W. Hasler, J. F. Kallehauge, R. H. Hansen, E. Samsøe, D. T. Arp, H. D. Nissen, J. M. Edmund, U. Bernchou, and F. Mahmood, Acta Oncol. **62**, 1551 (2023).

[13] I. Ranta, R. Kemppainen, J. Keyriläinen, S. Suilamo, S. Heikkinen, M. Kapanen, and J. Saunavaara, Phys. Med. **62**, 47 (2019).

[14] M. C. Schell, F. J. Bova, D. A. Larson, D. D. Leavitt, W. R. Lutz, E. B. Podgorsak, and A. Wu, AAPM Rep. 54, **1** (1995).

[15] E. Cirino, S. H. Benedict, P. J. Duepre, P. H. Halvorsen, G. G. Y. Kim, M. L. Reyhan, C. W. Schneider, L. Wang, C. P. Weaver, and S. Yoo, J. Appl. Clin. Med. Phys. **25**, 1 (2025).

[16] P. Y. Wen, M. van den Bent, G. Youssef, T. F. Cloughesy, B. M. Ellingson, M. Weller, E. Galanis, D. P. Barboriak, J. de Groot, M. R. Gilbert, R. Huang, A. B. Lassman, M. Mehta, A. M. Molinaro, M. Preusser, R. Rahman, L. K. Shankar, R. Stupp, J. E. Villanueva-Meyer, W. Wick, D. R. Macdonald, D. A. Reardon, M. A. Vogelbaum, and S. M. Chang, J. Clin. Oncol. **41**, 5187 (2023).

[17] B. M. Ellingson, M. Bendszus, J. Boxerman, D. Barboriak, B. J. Erickson, M. Smits, S. J. Nelson, E. Gerstner, B. Alexander, G. Goldmacher, W. Wick, M. Vogelbaum, M. Weller, E. Galanis, J. Kalpathy-Cramer, L. Shankar, P. Jacobs, W. B. Pope, D. Yang, C. Chung, M. V. Knopp, S. Cha, M. J. van den Bent, S. Chang, W. K. Yung, T. F. Cloughesy, P. Y. Wen, M. R. Gilbert, and Jumpstarting Brain Tumor Drug Development Coalition Imaging Standardization Steering Committee, Neuro Oncol. **17**, 1188 (2015).

[18] D. Grishchuk, A. Dimitriadis, A. Sahgal, A. D. De Salles, L. Fariselli, R. Kotecha, M. Levivier, L. Ma, B. E. Pollock, J. Régis, J. Sheehan, J. Suh, S. Yomo, and I. Paddick, Pract. Radiat. Oncol. **13**, 183 (2023).

[19] F. Putz, M. Bock, D. Schmitt, C. Bert, O. Blanck, M. I. Ruge, E. Hattingen, C. P. Karger, R. Fietkau, J. Grigo, M. A. Schmidt, T. Bauerle, and A. Wittig, Strahlenther. Onkol. **200**, 1 (2024).

[20] M. Niyazi, N. Andratschke, M. Bendszus, A. J. Chalmers, S. C. Erridge, N. Galldiks, F. J. Lagerwaard, P. Navarria, P. Munck Af Rosenschöld, U. Ricardi, M. J. van den Bent, M. Weller, C. Belka, and G. Minniti, Radiother. Oncol. **184**, 109663 (2023).

[21] R. Bitar, G. Leung, R. Perng, S. Tadros, A. R. Moody, J. Sarrazin, C. McGregor, M. Christakis, S. Symons, A. Nelson, and T. P. Roberts, RadioGraphics **26**, 513 (2006).

[22] K. Zhang, A. Ganjizadeh, S. Vahdati, J. Huston, M. A. Bernstein, B. J. Erickson, and Y. Shu, Radiology **315**, e241904 (2025).

[23] J. P. Marques, F. F. J. Simonis, and A. G. Webb, J. Magn. Reson. Imaging **49**, 1528 (2019).

[24] M. E. Molitch, JAMA **317**, 516 (2017).

[25] N. T. Jiam, D. M. Gillard, R. A. Morshed, A. S. Bhutada, E. D. Crawford, S. W. Braunstein, J. Henderson Sabes, P. V. Theodosopoulos, and S. W. Cheung, Laryngoscope Investig. Otolaryngol. **7**, 2057 (2022).

[26] M. T. Lawton, W. C. Rutledge, H. Kim, C. Stapf, K. J. Whitehead, D. Y. Li, T. Krings, K. terBrugge, D. Kondziolka, M. K. Morgan, K. Moon, and R. F. Spetzler, Nat. Rev. Dis. Primers **1**, 15008 (2015).

[27] G. Cruccu, G. Di Stefano, and A. Truini, N. Engl. J. Med. **383**, 754 (2020).

[28] D. Kondziolka, J. Neurosurg. **130**, 1789 (2019).

[29] T. Koga, M. Shin, and N. Saito, Neurol. Med. Chir. (Tokyo) **50**, 737 (2010).

[30] A. A. F. De Salles, A. A. Gorgulho, J. L. Pereira, and N.

McLaughlin, Neurosurg. Clin. N. Am. **24**, 491 (2013).
[31] J. P. Sheehan, C. P. Yen, C. C. Lee, and J. S. Loeffler, J. Clin. Oncol. **32**, 2836 (2014).
[32] Ministry of Health and Welfare of the Republic of Korea, Status of MRI Ownership by Province over the Past 5 Years (Ministry of Health and Welfare, Sejong, Republic of Korea, 2022).
[33] M. A. G. Ballester, A. P. Zisserman, and M. Brady, Med. Image Anal. **6**, 389 (2002).
[34] N. A. Koc, M. Rakowski, A. Dębska, B. Szmyd, A. Zawadzka, K. Zaczkowski, M. Podstawka, D. Wilmańska, A. Dobek, L. Stefańczyk, D. J. Jaskólski, K. Wiśniewski, Biomedicines **14**, 333 (2026).
[35] K. Malejko, S. Hafner, R. C. Brown, P. L. Plener, G. Grön, H. Graf, and B. Abler, Biomedicines **10**, 3188 (2022).
[36] S. Y. Huang, R. T. Seethamraju, P. Patel, P. F. Hahn, J. E. Kirsch, and A. R. Guimaraes, RadioGraphics **35**, 1439 (2015).